Published in final edited form as:
J Am Chem Soc. 2010 February 17; 132(6): 1929–1938. doi:10.1021/ja908139y.

Self-assembly synthesis, tumor cell targeting, and photothermal capabilities of antibody-coated indocyanine green nanocapsules

Jie Yu[1], **David Javier**[2], **Mohammad A. Yaseen**[3], **Nitin Nitin**[2], **Rebecca Richards-Kortum**[2], **Bahman Anvari**[4], and **Michael S. Wong**[1,5,*]

[1] Department of Chemical and Biomolecular Engineering, Rice University, Houston, TX 77251, USA

[2] Department of Bioengineering, Rice University, Houston, TX 77251, USA

[5] Department of Chemistry, Rice University, Houston, TX 77251, USA

[3] Department of Radiology, Massachusetts General Hospital, Charlestown, MA, 02129

[4] Department of Bioengineering, University of California, Riverside, CA, 99251, USA

Abstract

New colloidal materials that can generate heat upon irradiation are being explored for photothermal therapy as a minimally invasive approach to cancer treatment. The near-infrared dye indocyanine green (ICG) could serve as a basis for such a material, but its encapsulation and subsequent use is very difficult to carry out. We report the three-step room-temperature synthesis of ~120-nm capsules loaded with ICG within salt-crosslinked polyallylamine aggregates, and coated with anti-epidermal growth factor receptor (anti-EGFR) antibodies for tumor cell targeting capability. We studied the synthesis conditions such as temperature and water dilution to control the capsule size and characterized the size distribution via dynamic light scattering and scanning electron microscopy. We further studied the specificity of tumor cell targeting using three carcinoma cell lines with different levels of EGFR expression, and investigated the photothermal effects of ICG containing nanocapsules on EGFR-rich tumor cells. Significant thermal toxicity was observed for encapsulated ICG as compared to free ICG at 808 nm laser irradiation with radiant exposure of 6 W/cm^2. These results illustrate the ability to design a colloidal material with cell targeting and heat generating capabilities using non-covalent chemistry.

Keywords

cancer; charge assembly; encapsulation; near infrared; nanoparticles; polyallylamine

*Address correspondence to mswong@rice.edu.

Supporting Information Available

Complete Ref. [53]; Discussion of particle size distribution measurement analysis; Discussion of analysis of particle size distribution of Table 1; Figure S1 (Schematic of NIR laser irradiation of 1483 cells after the incubation with different formulations of ICG); Figure S2 (Calculated fractions of phosphate species at different pH values and measured electrophoretic mobility values for PAH/phosphate aggregate suspensions as a function of R ratio); Figure S3 (Size distributions of PAH/phosphate aggregates at different aging times); Figure S4 (Effect of deionized water on PAH/phosphate aggregate growth at 20°C); Figure S5 (Confocal microscopy of 1483 and SiHa cells without antibody or nanocapsule incubation) and Figure S6 (Fluorescence images of IgG-coated, ICG-containing nanocapsules and microcapsules). This material is available free of charge via the Internet at http://pubs.acs.org.

INTRODUCTION

Photothermal therapy (PTT) of cancer is extensively investigated as an alternative procedure to the traditional approaches such as surgery and chemotherapy.[1–5] In PTT, heat is generated within the targeted carcinoma tissue through absorption of the applied laser light, leading to thermal injury and cell death. Selective thermal injury to the targeted cancerous tissue without damaging the normal tissue structures remains one of the major challenges in PTT. Efforts have been made to increase the light sensitivity of targeted tissue through the use of exogenous chromophores such as gold nanoparticles (NPs),[6] gold nanorods[7], gold nanoshells (silica particles coated with a nanometer-thick gold shell),[2, 4] organic chromophores like indocyanine green (ICG),[8–10] and silver NP/organic dye composites,[11, 12] to increase heat generation within the targets. Given that these chromophores absorb light in the near infrared (NIR) region of the electromagnetic spectrum, they offer the advantage of increased penetration depth of the incident light since biological tissues are relatively transparent in NIR.[13]

ICG is FDA-approved for a number of clinical imaging applications[10, 14–17] and is under investigation in various PTT studies.[18–21] Current method of administering ICG is by dissolving it into saline and delivering it intravenously. Despite its clinical usage, ICC in its current formulation suffers from several major drawbacks: (1) concentration of the ICG solution and the nature of solvent have a significant influence on its absorption properties;[9, 22, 23] (2) ICG is an unstable molecule with temperature and light dependent optical properties;[9, 24, 25] (3) after a bolus intravenous injection, ICG binds readily to albumin and high-density lipoproteins (HDLs) in blood plasma such as alpha-1 lipoprotein, resulting in a red-shift in its optical absorption and subsequent alterations in its fluorescence emission properties;[26, 27] (4) ICG is non-selective for cancer cells; and (5) ICG is cleared rapidly from the body with a bi-exponential plasma clearance with a short half-life on the order of 2–4 minutes.[8, 17, 28] While the detailed mechanisms of ICG removal from body is not clearly understood, it is mainly eliminated from the general circulation by the liver, and excreted into the bile. It is not metabolized in the body; not reabsorbed from the small intestine; and does not undergo enterohepatic recirculation.[29] The short circulation time of ICG and its exclusive uptake by the liver greatly limit the potential of this non-toxic and clinically proven optical probe. With such limitations, use of ICG in both optical imaging and phototherapy of vascular malformations as well as targeting various tissues remains restricted.

To address these limitations, we recently reported the synthesis of ICG-containing nano/microcapsules through a modification of the process termed “tandem assembly” or “nanoparticle assembly”.[30] Aqueous solutions of polyallylamine hydrochloride (PAH) and dihydrogen phosphate salt are mixed together to form spherical aggregates onto which other coating materials such as dextran, poly-l-lysine, and magnetite nanoparticles can be deposited.[31, 32] This two-step tandem assembly process is in general suitable for non-destructive encapsulation of water-soluble compounds. Encapsulation of ICG[30] and other molecules[33, 34] requires an additional step, in which the molecule is introduced after the polyelectrolyte and salt are mixed together and before the coating materials are added. PAH is used as a model cationic polymer for ICG encapsulation due to its lower cost and well-established self-assembly chemistry, even though it is not generally considered a biocompatible material. An earlier study found that it can be non-toxic to rat fibroblast cells.[30]

Capsule sizes controlled within a range of 60–2000 nm, ICG content as high as 23% by dry weight, and minimal ICG leakage at room temperature and moderated leakage (17% loss of ICG) at 37 °C were found. Encapsulation shielded ICG from optical and thermal degradation when exposed to non-ambient light and temperature conditions for up to four days.[31] Experiments involving recurring laser irradiation of ICG-containing nanocapsules showed that they reached the same peak temperature multiple times, indicating ICG in encapsulated form

was less susceptible to photothermal degradation than free ICG.[30] Other ICG encapsulation methods using poly-lactic co(glycolic)-acid particles, phospholipid emulsions, silica NPs, and calcium phosphate NPs have been successfully demonstrated, but these synthesis methods either involved multiple processing steps or used toxic organic solvents and volatile monomers; the materials themselves have a lower ICG content than our charge-assembled ICG-containing capsules.[35–40] The advantages of our approach are that it takes only a few minutes for synthesis, it involves water and inexpensive reagents, and the processing occurs at room temperature and mild pH values. Previous studies indicated that it is possible to alter the biodistribution of ICG when it is delivered in an encapsulated formulation.[35] Our group showed that different coating materials can further modulate ICG biodistribution.[32]

To achieve effective PTT, the encapsulated ICG needs to be delivered to the targeted area. One approach in directing nanoconstructs to cancerous tissue capitalizes on the enhanced permeability and retention (EPR) effect[41, 42] where the endothelial walls of tumor vasculature are characterized by enlarged pore size.[43, 44] We chose a capsule diameter of ~100 nm as the target size, which is in the appropriate range for effective transport through the circulation system and for EPR.[45]

In addition to this passive targeting to the tumors, active targeting involving ligand-conjugated capsules that target specific receptors on the cancer cells can be investigated as a second approach.[46–49] Specifically, EGFR (epidermal growth factor receptor) is over-expressed on malignant cell surfaces such as breast, cervical, lung, and prostate cancer cells,[50–54] allowing for capsules coated with anti-EGFR antibodies (anti-EGFR, which is FDA-approved for use as a breast cancer therapeutic agent[55]), to bind preferentially over non-cancer cells.

In this paper, we report on the tandem, or step-wise, assembly synthesis of ~120-nm capsules containing ICG and coated with anti-EGFR, and their ability to target and induce photothermal injury to cancer cells *in vitro*. We present the effects of charge ratio *R*, synthesis temperature and time, dilution of the PAH/phosphate aggregates, and ICG content on capsule size control. We refer to these ICG-containing, anti-EGFR-coated capsules as “nanocapsules.” While nanoparticles have diameters strictly between 1 and 100 nm, submicron particles (with diameters of several hundred nanometers) are occasionally called “nanoparticles” in biomedical applications.[56] This work represents the first demonstration of the dual functionality of ICG-containing constructs for targeting and photothermal treatment of cancerous cells.

EXPERIMENTAL METHODS

Materials

Poly(allylamine hydrochloride) (“PAH,” 70,000 g/mol, chloride counterion, Sigma-Aldrich), disodium hydrogen phosphate heptahydrate ($Na_2HPO_4{\cdot}7H_2O$, 99.5%, Fisher), and indocyanine green (ICG, ~90%, powder, Sigma-Aldrich) were used as received. The B-cell hybridoma for monoclonal EGFR antibody (MAB-108) production was produced and purified using the Baylor College of Medicine Monoclonal Antibody Core Facility (Houston, TX). IgG antibody (from rabbit serum) and fluorescein isothiocyanate conjugated antibody (FITC-IgG antibody; from rabbit serum) were purchased from Sigma-Aldrich and dissolved in deionized water (18.2 M, Barnstead Nanopure Diamond System) for use. Stock solutions of PAH, Na_2HPO_4, and ICG were prepared using 4 °C deionized water, and stored at 4 °C before use. Phosphate buffered saline (PBS) solution (0.01 M Na_2HPO_4, 0.138 M NaCl, 0.0027 M KCl, pH = 7.4) was prepared by dissolving pre-made powder (Sigma-Aldrich) in deionized water directly. Trypan blue solution (0.4%) was purchased from Sigma-Aldrich (MI, USA) and diluted to 0.1% with deionized water before use.

For the *in vitro* study, hybridoma cell lines 1483, SiHa, and 435 were used as model systems for anti-EGFR targeting. The cell lines were purchased from ATCC (American Type Culture Collection) and cultured using recommended media and conditions. DMEM (Dulbecco's minimum essential media) with 5% FBS (Fetal Bovine Serum) with antibiotics were used. Two types of cell cultures were used: cell suspensions prepared from trypsin treatment of the attached cells and re-dispersed in PBS solution (cell concentration was ~10^6/ml); and cells grown on glass substrates. The first type cell was used for confocal microscopy and the latter one was used for laser irradiation. Fresh medium was used before incubating with ICG-nanocapsules. The cell density was ~10^4/cm^2.

Synthesis of ICG-containing nanocapsules and conjugation of anti-EGFR

In a typical synthesis, cooled PAH solution (4 °C, 2 mg/ml, 20 μl, pH = 4.3) was vortexed with pre-cooled Na_2HPO_4 solution (4 °C, 0.005 M, 120 μl) at room temperature. PAH/phosphate aggregates formed upon mixing. Then 1.2 ml of cooled deionized water (4 °C, 18.2 M, Barnstead Nanopure Diamond System) was added to the PAH/phosphate aggregate suspension immediately, followed by the addition of 120 μl of cooled ICG aqueous solution (4 °C, 1 mg/ml). All mixing times were 10 sec. The ratio of total negative charge of the added salt to the total positive charge of the polymer, or the *R* ratio, was set at 3. The resultant suspension was aged for 2 hours at 4 °C, then washed twice with PBS solution through centrifugation (3000 rpm for 2 hr) and re-dispersed in the same volume of PBS solution.

Anti-EGFR-coated ICG-containing nanocapsules were prepared by adding the diluted antibody solution (500 μl, 20 μg/ml) to 300 μl of the washed ICG-containing aggregate suspension (ICG concentration of 0.05 mg/ml) and aged overnight at 4 °C. The uncoated aggregate suspension was stored at 4 °C, to be used as the uncoated nanocapsules. The coated nanocapsules were recovered via the same two centrifugation cycles and redispersed in 800 μl of PBS solution. Unless stated otherwise, the capsules were re-suspended in PBS solution. IgG was used as a control antibody in our cell photothermal studies. The same amount of IgG antibody molecules were added to the ICG-containing aggregate suspension, aged and washed under the same condition.

To prove the presence of encapsulated ICG and the IgG shell, capsules were synthesized using the following recipe: PAH = 2 mg/ml, R = 6, 20 °C, no dilution and the PAH/phosphate aggregates were aged for 30 min before ICG was added. The PAH/salt/ICG aggregates were washed after 2 hr of aging, after which IgG was added and then aged for 2 hr.

ICG loading efficiency and content determination

The amount of ICG loaded into the nanocapsules was determined before anti-EGFR addition. One batch of ICG-nanocapsules was centrifuged and the supernatant was carefully removed and stored in a 1.7 ml centrifuge tube; the capsules were dispersed in PBS solution. The centrifugation was repeated, and the collected supernatant was combined with the other supernatant volume. The ICG concentration in the supernatant was quantified via UV-vis spectroscopy when diluted 600 times with pH 14 PBS solution. ICG decay was found to be negligible at the ICG concentrations measured, consistent with published reports of ICG stability at high concentrations in water.[25] ICG inside the aggregates were also measured in a similar manner to check the accuracy of the above method. Selected samples of ICG-nanocapsules were treated with high pH solution (pH ~13–14) to induce capsule disassembly and ICG release into solution.[57] For all samples tested, the amount of incorporated ICG and unincorporated ICG equaled the initial precursor ICG, indicating mass balance was closed. Measurements were performed at least 3 times to ensure reproducibility.

Cell targeting

200 μl of the cell suspension was mixed with 200 μl of antibody-coated ICG-nanocapsules ([ICG] = 0.08 mg/ml in the whole suspension, ~10^8 particles/ml). The mixture was stored in an incubator for 30 min at 37 °C, and then washed with PBS through low-speed centrifugation to remove unconjugated ICG-nanocapsules. For confocal microscopy, 10 μl of the resulting cell pellet was spread on a glass slide and sealed by glass cover. The remaining cell suspension was then fixed with formalin solution (10 wt%) and washed with deionized water, then dried and sputter coated with Au for SEM imaging. As a control, 200 μl of uncoated nanocapsules was added to 1483 cells and incubated under the same conditions, and then washed. The same method was applied to IgG-coated nanocapsules when they were incubated with 1483 cells.

In vitro photothermal experiments

For laser irradiation experiment, the cell was immobilized on a glass surface during the culture in DMEM (Dulbecco's minimum essential media) containing 5% FBS (Fetal Bovine Serum). The cell density was $10^4/cm^2$. Washed anti-EGFR coated ICG-particles were concentrated by 30x factor, resulting in [ICG] = 0.4 mg/ml in the suspension. A small amount of the suspension (0.02 ml, ~10^9 particles/ml, ~10^{11} ICG molecules/particles, 0.04 wt% ICG of suspension) was added into 1483 cells. 20 μl of either ICG solution or non-coated ICG-nanocapsules were added into the cell chambers as control samples. After 30 min incubation at 37 °C, the old medium and unbound ICG or ICG-nanocapsules were removed and fresh medium (DMEM with 5% FBS) was added. Selected areas (Fig. S1) were irradiated with a continuous-wave near-infrared diode laser (Coherent FAP-System, λ = 808 nm) with a 6 mm diameter laser spot and adjusted power as given in the text for 200 seconds.

After irradiation, cells were restored in incubator for another 2 hours. To assess cell injury, irradiated cells were washed with sterilized PBS solution once and merged with 0.5 ml of PBS solution, followed by the addition of 0.5 ml of trypan blue staining solution (0.1 wt%). Trypan blue dye molecules easily penetrate the plasma membrane of dead cells to stain the nuclei; viable cells were unstained.

Characterization

Scanning electron microscopy (SEM) images were performed with FEI XL-30 environmental SEM operating at 30 kV with a working distance of 10.0 mm. The nanocapsules were washed twice with deionized water, loaded on a SEM stub, dried under air overnight, and sputter-coated with gold before SEM imaging. Confocal images were taken with a Zeiss LSM 510 confocal microscope. The size distribution of capsules in the dry state was obtained by measuring the diameters of 500 particles using the ImageJ software.[58]

Absorbance spectra of ICG solution and ICG-nanocapsules suspension were performed using a UV-vis spectrometer (Shimadzu, UV2401-PC model). The samples were handled in a low-light environment to minimize ICG interactions with ambient light.

The hydrodynamic diameter of polymer aggregates was measured through dynamic light scattering (DLS, Brookhaven, ZetaPALS with BI-9000AT digital autocorrelator, λ = 656 nm). The measurements started immediately after PAH and salt solution was mixed (time = 0). The two common mathematical models to fit the autocorrelation function (ACF) are NNLS (Non-Negatively constrained Least Squares) and CONTIN. With NNLS providing better fits for multimodal distributions and CONTIN being more accurate for a unimodal distribution, the latter was used.[59]

The electrophoretic mobilities of uncoated and antibody-coated ICG-containing nanocapsules were measured by phase analysis light scattering (PALS) using the ZetaPALS setup. A dip-in

(Uzgiris type) electrode system with 4 ml polystyrene cuvette was used, and measurements were taken at 6 °C (the lowest temperature available for the instrument).

Free chloride ion concentrations was measured with a Chloride Ion Selectivity meter (Thermo Orion model 720A Plus bench-top meter) and a chloride Ionplus electrode (Orion Cat. No. 9617BN) at room temperature.

RESULTS AND DISCUSSIONS

Controlling nanocapsule size by studying polymer/salt aggregate growth

Effect of R ratio—The three-step process for synthesizing ICG-containing nanocapsules (ICG-NC's) with anti-EGFR coating is shown in the experimental methods (Scheme 1). In this synthesis, counterion condensation drives the electrostatic crosslinking between the PAH chains and the phosphate anions.[30, 60]

The PAH solution contained free chloride anions, representing approximately 25% of the chloride counterions of the polymer. In the presence of phosphate, the free chloride concentration increased (Fig. 1a), indicating that the phosphate drove the release of the bound chloride counterion. Increasing the *R* ratio (the ratio of total negative charge of the added salt to the total positive charge of the polymer) led to higher free chloride concentrations and eventually to the formation of polymer/salt aggregates. Aggregate formation was observed at $R > 0.6$, where most of the chloride counterions (~90%) was released and replaced by the phosphate ions with the multivalency necessary for crosslinking PAH chains.[60, 61] pH values of the PAH/phosphate mixtures increased from 4 to 9 as the *R* ratio increased from 0 to 10 (due to increasing amounts of Na_2HPO_4 solution added). The pH changed little above $R = 2$, in which the majority species were monohydrogen phosphate (HPO_4^{2-}, Fig. S2(a)). To remove any pH effects on aggregate formation, subsequent experiments were carried out at $R = 2$ and above.

It was previously reported that, once formed, the polymer/salt aggregates grew in size with time, depending on the *R* ratio.[60] For the PAH/phosphate system, the small *R* ratio of 2 led to aggregates that were small and stable in size, and larger *R* ratios between 6 to 10 led to larger and fast growing aggregates(Fig. 1b). The growth rate trend was correlated to the electrophoretic mobility of the polymer/salt aggregates (Fig. S2(b)). Higher *R* ratios led to aggregates with decreasing electrophoretic mobilities and less positively charged surface, which then led to reduced electrostatic repulsion among the aggregates and increased growth rates, following the Derjaguin-Landau-Verwey-Overbeek theory (DLVO theory) of colloidal stability.[62]

Size distribution analysis of PAH/phosphate aggregates—To eliminate size-dependent effects on particle uptake by cells and tissue, it was important that the capsules (and therefore the polymer/salt aggregates) be as narrow in size as possible.[63] In this work, R = 3 was chosen for the detailed size analysis on PAH/phosphate aggregate. The growth curves in Fig. 1b showed intensity-weighted average hydrodynamic diameters but provided no information on size distribution, though. A careful size distribution analysis was thus performed at several aging times (Table 1, Fig. S3). A comparison of the intensity-based and number-based average diameters indicated that the aggregate size distribution broadened with time. We favored short aging times over long aging times, as judged from the RSD and PDI values (a detailed discussion is located in Supporting Information).

Producing smaller polymer/salt aggregates—We found that dilution slowed down aggregate growth (Fig. 2, S4). Water was added (such that the PAH/phosphate concentration was reduced by 10 times) 6 min after the PAH/phosphate aggregate formation at 20 °C, which

resulted in an immediate reduction in growth rate and average size of ~220 nm at 30 min (Fig. 2a). Without this delayed dilution, the aggregates grew to be ~280 nm at 30 min. Immediate dilution with the same amount of water after the PAH/phosphate aggregate formation led to smaller aggregate sizes of ~150 nm (Fig. 2b).

We found that aging temperature also slowed down aggregate growth. Using precursor solutions of PAH and phosphate refrigerated at 4 °C, we prepared aggregates within 30 sec and performed low-temperature DLS measurements at 6 °C immediately. Measurements were not done at 4 °C due to equipment limitations. The PAH/phosphate aggregates were ~115 nm when grown at 6 °C, which was less than half the size produced at 20 °C, and were even smaller (at ~100 nm) at 6 °C and after 10× dilution (Fig. 2c). Thus, we chose the synthesis conditions of $R = 3$, cooled PAH and phosphate precursor solutions, immediate 10× dilution of the aggregate suspension, and aging temperature of 4 °C (refrigerator temperature).

Size effect of ICG inclusion—We found that ICG addition also affected aggregate growth behavior. As shown in our previous studies, ICG was encapsulated by combining a free solution of ICG with the polymer/salt aggregate suspension.[30] The amount of ICG used was chosen to be ICG/amine = 0.36 so that the resulting aggregates had a high ICG content and high colloidal stability. Combining ICG immediately after PAH/phosphate aggregate formation resulted in an immediate reduction in growth rate and a fairly stable size of ~190 nm (Fig. 2a). Delayed dilution with water at 6 min led to a slight decrease of ~10 nm. Adding the same amount of water immediately after the PAH/phosphate aggregate formation and then adding ICG led to a further decrease to ~120 nm, indicating a contraction of ~35 nm or 37% (Fig. 2b). The aggregates contracted to 100 nm when they were aged at the lower temperature of 6 °C and ICG was added immediately (Fig. 2c). Dilution of the aggregate suspension aged at 6 °C followed by ICG addition reduced aggregate sizes slightly more, to ~90–95 nm (Fig. 2c); thus, we adopted this as our part of the ICG nanocapsule synthesis protocol.

As a negatively charged dye molecule, ICG interacted with the polymer/salt aggregates electrostatically, and stabilized the PAH/phosphate aggregate particulate structure through its incorporation throughout the aggregate. Interestingly, while average sizes were comparable, the size distributions were not. At 6 °C and without ICG, the PAH/phosphate aggregates were bimodal after 30 min whereas ICG-containing aggregates were unimodal and monodisperse (PDI = 0.002) (Fig. 2d). We concluded that long aging times favored aggregate growth, size broadening and the formation of two different-sized aggregates, and that the presence of ICG favored smaller, uniform aggregates.

Anti-EGFR shell formation

These PAH/phosphate/ICG aggregates were sufficiently stable against precipitation that we considered these to be uncoated nanocapsules, minus the shell. After contacting with anti-EGFR, the thus-coated ICG-containing nanocapsules were analyzed through SEM (Fig. 3). The uncoated and coated ones had average sizes of 96 nm (RSD = 11%) and 110 nm (RSD = 23%), respectively. This indicated that the anti-EGFR coating was 7 nm thick. anti-EGFR is a member of immunoglobulin G (IgG) antibody family, and it shares their molecular weight (150 kDa) and flexible Y-shape protein conformation.[46, 64, 65] From structural calculations by Pease *et al.*,[66] the arms and stem of the IgG "Y" are 8.9 nm and 7.7 nm long, respectively, the thickness is 4.0 nm, and the diameter of the equivalent aerodynamic sphere is 9.4 nm. Anti-EGFR is expected to have these dimensions also, consistent with the anti-EGFR shell thickness of the capsules.

Through DLS, uncoated and anti-EGFR-coated nanocapsules were characterized in the un-dried, suspended state (Fig. 3c, f). The uncoated and coated ones had average hydrodynamic diameters of 106 nm (RSD = 5%) and 122 nm (RSD = 15%), respectively, giving a shell

thickness of 8 nm. These values were larger than the SEM measurements, indicating a contraction of 9–10% after drying. The anti-EGFR coating broadened the size distribution of the uncoated nanocapsules (the polymer/salt/ICG aggregate) even though the shell was only protein thick. This would be consistent with a randomized orientation of the non-spherical anti-EGFR antibodies on the aggregate surface, in which capsules could have slightly larger diameter if some anti-EGFR attached to the surface at the tips of the arms or stem.

The ICG loading of the uncoated nanocapsules was 36% by dry weight, and overall ICG encapsulation efficiency was 56%. No room-temperature ICG leakage was detected after one week. The anti-EGFR shell added <1% to the total capsule weight, and so the ICG loading content remained at 36%. No ICG leakage was detected during the anti-EGFR shell formation or during the cell culture studies.

Measured at pH = 7.4 in PBS buffer solution, the uncoated and coated nanocapsules respectively had zeta potential values of −5.8 mV and −5.4 mV and electrophoretic mobilities of $-0.20\ \mu m \cdot cm^{-1} \cdot V^{-1}$ and $-0.19\ \mu m \cdot cm^{-1} \cdot V^{-1}$), indicating a net negative surface charge for both materials. These results further indicated that the anti-EGFR (which had an estimated isoelectric point of 6.1[67]) negligibly changed the surface charge. The shell formation resulted from charge interactions between the carboxyl groups of anti-EGFR molecule and amine groups of the PAH chains of the uncoated nanocapsules similar to anti-EGFR charge interactions with amine group-modified Au NPs.[68]

State of encapsulated ICG

Macroscopically, the anti-EGFR-coated ICG-nanocapsule suspension was slightly green and clear, similar to a free ICG solution (Fig. 4a, d). The non-ICG-containing PAH/HPO_4^{2-} aggregate suspension had no color (Fig. 4e). The nanocapsules settled after 3 days (Fig. 4b), consistent with their small zeta potential value. They were readily re-suspended after manual agitation or sonication (Fig. 4c). They could also be centrifuged at 3000 rpm for 2 hr without damage, to produce a precipitate that is readily re-suspended. Leakage of ICG was negligible after re-suspension in a PBS solution, as shown previously.[30]

It is necessary to assess the extent of shifting in absorbance spectrum once ICG is encapsulated. The ICG-containing nanocapsules exhibited relatively strong absorbance in the NIR range (>750 nm) with the two broad peaks red-shifted from those in the free ICG spectrum (Fig. 4e). Red-shifts have been reported for cases in which ICG binds to plasma in blood[36] or ICG form molecular aggregates at high concentrations in water.[69] The observed red-shift (~70 nm) indicated the ICG local environment was different within the capsules compared to that of free ICG, and interestingly, it was more severe than our previous measurements on larger ICG-containing capsules (1–2 μm), which had a red-shift of ~50 nm. This difference may have been the result of much higher local concentrations of ICG within the smaller nanocapsules: ~50 g/(mL of nanocapsule volume) compared to ~13 g/(mL of microcapsule volume), which correspond to 36 wt% and 14 wt% ICG, respectively. The 36 wt% ICG of our nanocapsules exceeds the ICG content of other encapsulation materials reported: for example, 0.3 wt% for poly-lactic co(glycolic)-acid particles,[70] 0.3 wt% for phospholipid emulsions,[38] 3 wt% for silica NPs,[39] and ~17 wt% ICG for calcium phosphate NPs.[40] ICG absorbance decreased after encapsulation by 25% at 700 nm and 35% at 780 nm, but it did not change much at 630 nm (excitation wavelength used in laser confocal microscopy = 633 nm) or at 800 nm (excitation wavelength used in photothermal cell culture tests = 808 nm).

Cell targeting by anti-EGFR-coated ICG-containing nanocapsules

To investigate the binding ability of anti-EGFR-coated ICG-nanocapsules, we used three carcinoma cell lines, 1483 (human head and neck squamous cell), SiHa (human cervical

squamous cell), and 435 (cancerous human breast cell) with various expression levels of EFGR. We ensured that the nanocapsule amount added was commensurate with the total EGFRs available for binding, by estimating that each 122-nm capsule carried a maximum of ~500 antibody molecules. With a capsule concentration of ~10^8 particles/mL and volume of 0.2 mL used, and cell density of 10^6 cell/mL and volume of 0.2 mL, 5×10^4 anti-EGFRs were available for each cell. This number is in the range of EGFRs content (10^4–10^6 #/cell) for most carcinomas cells.[71] As expected, nanocapsules (identified by their ICG fluorescence) were detected along the cell periphery (Fig. 5). No fluorescence was found in cells incubated in the absence of nanocapsules or free anti-EGFR (Fig. S5).

Whereas 1483 and SiHa cells have similar amounts of EGFRs on their surface (10^5–10^6 #/cell), receptors on 435 cells are ten times less expressed. Analyzed through ImageJ,[58] the red rings in 1483 and SiHa cells were more intense than the ones in 435 cells (Fig. 5d), which indeed showed the 1483 and SiHa cell surfaces to be enriched with the nanocapsules.

SEM provided additional support of nanocapsule binding to the cell surfaces, with a comparison of untreated cells to those treated with the capsules indicating a distinct difference in surface roughness (Fig. 6). Features with ~100 nm sizes were found on the surface of 1483 and SiHa cells, consistent with the nanocapsules. None were found on the 435 cells, which was consistent with its lower EGFR surface density and lower capsule content.

To compare the binding affinity of antibody-coated nanocapsules with uncoated nanocapsules, we chose 1483 cells as the model system. Based on fluorescence intensity profiles, comparable amounts of uncoated nanocapsules also associated with the cells, likely due to charge interactions between the PAH amine groups of uncoated nanocapsule surface and the negative cell membrane (Fig. 7). We then prepared nanocapsules coated with IgG (which are not selective for EGFR binding), and found that there was less attachment to the cells (Fig. S6). It was concluded that uncoated nanocapsules can bind to cells, and this binding can be controlled by the nature of the coating material.

Photothermal testing of anti-EGFR-coated ICG-containing nanocapsules

Previously we demonstrated the heat generating capabilities of ICG-containing microcapsules in PBS suspension[30] and in a gelatin phantom simulating tumorous tissue.[72] Similar testing with this material had not been performed on live cells. Here, we used the 1483 cells of the 3 cell lines as a model system since they contained the highest levels of EGFR expression, and 3 formulations of ICG (free ICG in PBS solution, uncoated ICG-containing nanocapsules, and anti-EGFR-coated ones).

Figure 8 showed the effects of ICG formulation and NIR laser radiant exposure. For all cases, cell death was not observed if there was no irradiation. Without ICG, cell death was not observed at the irradiation exposure levels tested (Fig. 8a). Cells incubated with free ICG did not show any evidence of laser-induced hyperthermic injury either (Fig. 8b). There was an insufficient amount of ICG localized at the cell surface, which would have been due to the absorption of free ICG by the serum albumin in the medium rather by the cells. The antibody-coated nanocapsules, in contrast, caused cell death with irradiation, as observed by the trypan blue dye which stained the nuclei of dead cells (Fig. 8c). The uncoated nanocapsules also caused cell death with irradiation but to a lesser extent at 3 W/cm^2 (Fig. 8d), suggesting that these capsules absorbed non-specifically but sufficiently to the cell surface for some photothermal injury to occur. At 6 W/cm^2, significantly higher cell death was observed with both uncoated and antibody-coated nanocapsules.

More quantitatively, cell lethality at 3 W/cm^2 radiant exposure was 30–65% using anti-EGFR-coated nanocapsules and 10–50% using uncoated nanocapsules. Thus, photothermal efficacy

was improved by active targeting via antigen-antibody interactions. At 6 W/cm^2, cell lethality was 90–100% with the coated ones and 65–95% with uncoated nanocapsules. Nearly all the cells were destroyed, indicating the use of higher radiant exposures compensated for the non-specific and reduced cellular uptake of the uncoated capsules. With both formulations showing the ability to bind to 1483 cells, this observed higher cell lethality at 3 W/cm^2 could be attributed to the greater amount of bound anti-EGFR-coated capsules compared to the uncoated nanocapsules, consistent with confocal microscopy results (Fig. 7).

To provide some context to the temperatures experienced by the cells (which was not determined due to instrumentation limitations), we previously showed that a PBS suspension of silica NP-coated, ICG-containing microcapsules could be heated to 50 °C in 20 sec and to ~75 °C in 30 sec with NIR laser irradiation (λ = 808 nm) at an intensity of 155 W/cm.[30] The 70–80 °C temperature range is sufficiently high for cell death to occur, due to thermally-induced protein denaturation.[73] Further, we found that dextran-coated ICG-containing mesocapsules (500 nm) within a cylindrical-shaped gelatin sample which was embedded in a chicken breast sample led to a local temperature increase of 12 °C at a NIR laser intensity of 5.25 W/cm^2 after 200 sec.[72] Comparing laser power and irradiation times with values typically used with other nanomaterials, the 3 and 6 W/cm^2 intensities and 200 sec were lower than those used in *in vitro* photothermal studies of Au NPs (up to 64 W/cm^2, 240 sec) and gold nanoshells (80 W/cm^2, 420 sec).[3, 74]

CONCLUSIONS

We report a room-temperature, one-pot, all-water synthesis of a class of nanocapsular material with the demonstrated functions of cell targeting and photothermal heat generation. Careful light scattering studies indicated that monodisperse polymer/salt aggregates were achieved at a low charge ratio, low aging temperature, and dilution during growth. Short aging times were necessary for monodisperse size distributions unless ICG was incorporated into the PAH/phosphate aggregates, which also eliminated the synthesis condition of dilution. These ICG-containing aggregates can be coated by a single layer of anti-EGFR bimolecular via electrostatic conjugation, resulting in ~120-nm capsules that can bind to cancer cells. Selective binding was shown by their ability to distinguish cells of different EGFR expressions (1483 and SiHa cells versus 435 cells). Both anti-EGFR-coated and uncoated nanocapsules are capable of significant cell lethality, with the former showing greater performance due to higher local capsule concentrations resulting from selective binding. Through a more detailed understanding of the non-covalent self-assembly chemistry, the size, structure, and function of multicomponent capsular materials can be readily controlled.

Supplementary Material

Refer to Web version on PubMed Central for supplementary material.

Acknowledgments

This work was supported by National Science Foundation (CBET-0652073, MSW), a Smalley-Curl Innovation Award (MSW), 3M (Young Faculty Award, MSW), and National Institute of Health (GMO-8362, MAY; R01-AR47996, BA). We are grateful to Prof. J. L. West (Rice University) for use of the laser equipment and to Dr. P. Diagaradjane (M.D. Anderson Cancer Center, Houston) for valuable discussions.

References

1. Welch AJ. IEEE J Quantum Electrons 1984;QE-20:1471–1481.
2. Hirsch LR, Stafford RJ, Bankson JA, Sershen SR, Rivera B, Price RE, Hazle JD, Halas NJ, West JL. Proc Natl Acad Sci U S A 2003;100:13549–13554. [PubMed: 14597719]

3. El-Sayed IH, Huang XH, El-Sayed MA. Cancer Lett 2006;239:129–135. [PubMed: 16198049]
4. Gobin AM, Lee MH, Halas NJ, James WD, Drezek RA, West JL. Nano Lett 2007;7:1929–1934. [PubMed: 17550297]
5. Gu YQ, Chen WR, Xia MN, Jeong SW, Liu HL. Photochem Photobiol 2005;81:1002–1009. [PubMed: 15807632]
6. Jain PK, El-Sayed IH, El-Sayed MA. Nano Today 2007;2:18–29.
7. Huang XH, El-Sayed IH, Qian W, El-Sayed MA. J Am Chem Soc 2006;128:2115–2120. [PubMed: 16464114]
8. Taichman GC, Hendry PJ, Keon WJ. Texas Heart Ins J 1987;14:133–138.
9. Landsman MLJ, Kwant G, Mook GA, Zijlstra WG. J Appl Physiol 1976;40:575–583. [PubMed: 776922]
10. Benson RC, Kues HA. Phy Med Biol 1978;23:159–163.
11. Skirtach AG, Antipov AA, Shchukin DG, Sukhorukov GB. Langmuir 2004;20:6988–6992. [PubMed: 15301477]
12. Skirtach AG, Dejugnat C, Braun D, Susha AS, Rogach AL, Parak WJ, Mohwald H, Sukhorukov GB. Nano Lett 2005;5:1371–1377. [PubMed: 16178241]
13. Weissleder R. Nat Biotechnol 2001;19:316–317. [PubMed: 11283581]
14. Ntziachristos V, Yodh AG, Schnall M, Chance B. Proc Natl Acad Sci U S A 2000;97:2767–2772. [PubMed: 10706610]
15. Hollins B, Noe B, Henderson JM. Clin Chem 1987;33:765–768. [PubMed: 3594811]
16. Licha K, Riefke B, Ntziachristos V, Becker A, Chance B, Semmler W. Photochem Photobiol 2000;72:392–398. [PubMed: 10989611]
17. Desmettre T, Devoisselle JM, Mordon S. Surv Ophthal 2000;45:15–27.
18. Liu VG, Cowan TM, Jeong SM, Jacques SL, Lemley EC, Chen WR. Lasers Med Sci 2002;17:272–279. [PubMed: 12417982]
19. Chen WR, Adams RL, Bartels KE, Nordquist RE. Cancer Lett 1995;94:125–131. [PubMed: 7634239]
20. Chen WR, Adams RL, Bartels KE, Nordquist RE. Cancer Lett 1996;98:169–173. [PubMed: 8556705]
21. Tuchin VV, Genina EA, Bashkatov AN, Simonenko GV, Odoevskaya OD, Altshuler GB. Lasers Surg Med 2003;33:296–310. [PubMed: 14677157]
22. Philip R, Penzkofer A, Baumler W, Szeimies R-M, Abels C. J Photochem Photobiol A 1996;96:137–148.
23. Mordon S, Devoisselle JM, Soulie-Begu S, Desmettre T. Microvas Res 1998;55:146–152.
24. Holzer W, Mauerer M, Penzkofer A, Szeimies R-M, Abels C, Landthaler M, Baumler W. J Photochem Photobiol B 1998;47:155–164. [PubMed: 10093915]
25. Saxena V, Sadoqi M, Shao J. J Pharm Sci 2003;92:2090–2097. [PubMed: 14502548]
26. Dinsomre AD, Hus MF, Nikolaides MG, Marquez M, Bausch AR, Weitz DA. Science 2002;298:1006. [PubMed: 12411700]
27. Wolfe JD, Csaky KG. Exp Eye Res 2004;79:631–638. [PubMed: 15500822]
28. El-Desoky A, Seifalian AM, Cope M, Delpy DT, Davidson BR. Br J Surg 1999;86:1005–1011. [PubMed: 10460634]
29. Shinohara H, Tanaka A, Kitai T, Nobuharu Y, Inomoto T, Satoh S, Hatano E, Yamaoka Y, Hirao K. Hepatology 1995;23:137–144. [PubMed: 8550033]
30. Yu J, Yaseen MA, Anvari B, Wong MS. Chem Mater 2007;19:1277–1284.
31. Yaseen MA, Yu J, Wong MS, Anvari B. J Biomed Opt 2007;12:1–8.
32. Yaseen MA, Yu J, Wong MS, Anvari B. Opt Express 2008;16:20577–20587. [PubMed: 19065196]
33. Rana RK, Murthy VS, Yu J, Wong MS. Adv Mater 2005;17:1145–1150.
34. Murthy, VS.; Wong, MS. Enzyme encapsulation using Naoparticle-assembed capsules. Vol. 986. Oxford University Press; New York: 2008. p. 214-232.
35. Saxena V, Sadoqi M, Shao J. Int J Pharm 2006;308:200–204. [PubMed: 16386861]
36. Devoisselle JM, Soulie-Begu S, Mordon S, Desmettre T, Maillols H. Lasers Med Sci 1998;13:279–282.

37. Mordon S, Devoisselle JM, Begu S, Desmettre T. Lasers Med Sci 1998;13:181–188.
38. Yuan BH, Chen NG, Zhu Q. J Biomed Opt 2004;9:497–503. [PubMed: 15189087]
39. Kim G, Huang SW, Day KC, O'Donnell M, Agayan RR, Day MA, Kopelman R, Ashkenazi S. J Biomed Opt 2007;12:044020. [PubMed: 17867824]
40. Altinoglu AI, Russin TJ, Kaiser JM, Barth BM, Eklund PC, Kester MK, Adair JH. ACSNano 2008;2:2075–2084.
41. Hobbs SK, Monsky WL, Yuan F, Roberts WG, Griffith L, Torchilin VP, Jain RK. Proc Natl Acad Sci U S A 1998;95:4607–4612. [PubMed: 9539785]
42. Rejman J, Oberle V, Zuhorn IS, Hoekstra D. Biochem J 2004;377:159–169. [PubMed: 14505488]
43. Yuan F, Delian M, Fukumura D, Leuning M, Berk D, Torchilin VP, Jain RK. Cancer Res 1995;55:3752–3756. [PubMed: 7641188]
44. Jain RK, Munn LL, Fukumura D. Nat Rev Cancer 2002;2:266–276. [PubMed: 12001988]
45. Brigger I, Dubernet C, Couvreur P. Adv Drug Delivery Rev 2002;54:631–651.
46. Holliger P, Bohlen H. Cancer Metastasis Rev 1999;18:411–419. [PubMed: 10855784]
47. Nobs L, Buchegger F, Gurny R, Allemann E. J Pharm Sci 2004;93:1980–1992. [PubMed: 15236448]
48. Reddy GR, Bhojani MS, McConville P, Moody J, Moffat BA, Hall DE, Kim G, Koo YEL, Woolliscroft MJ, Sugai JV, Johnson TD, Philbert MA, Kopelman R, Rehemtulla A, Ross BD. Clin Cancer Res 2006;12:6677–6686. [PubMed: 17121886]
49. Charrois GJR, Allen TM. Biochim Biophys Acta 2003;1609:102–108. [PubMed: 12507764]
50. Saloman DS, Brandt R, Ciardiello F, Normanno N. Crit Rev Oncol/Hematol 1995;19:6550–6565.
51. Wright C, Mellon K, Johnston P, Lane DP, Harris AL, Horne CHW, Neal DE. Br J Cancer 1991;63:967–970. [PubMed: 1712624]
52. Santini J, Formento JL, Francoual M, Milano G, Schneider M, Dassonville O, Demard F. J Sci Special Head Neck 1991;13:132–139.
53. Paez JG, et al. Science 2004;304:1497–1500. [PubMed: 15118125]
54. Rusch V, Baselga J, Cordoncardo C, Orazem J, Zaman M, Hoda S, McIntosh J, Kurie J, Dmitrovsky E. Cancer Res 1993;53:2379–2385. [PubMed: 7683573]
55. Pfeiffer D, Stellwag B, Pfeiffer A, Borlinghaus P, Meier W, Scheidel P. Gynecol Oncol 1989;33:146–150. [PubMed: 2784777]
56. Letchford K, Burt H. Eur J Pharm Biopharm 2007;65:259–269. [PubMed: 17196803]
57. Murthy VS, Cha JN, Stucky GD, Wong MS. J Am Chem Soc 2004;126:5292–5299. [PubMed: 15099114]
58. ImageJ. 2005. p. 34http://rsb.info.nih.gov/ij/
59. Brown, W. Dynamic Light Scattering, the Method and Some Application. Clarendon Press; Oxford: 1993.
60. Murthy VS, Rana RK, Wong MS. J Phys l Chem B 2006;110:25619–25627.
61. Bosshard HR, Marti DN, Jelesarov I. J Mol Recognit 2004;17:1–16. [PubMed: 14872533]
62. Hunter, RJ. Foundations of Colloids Science. Oxford University Press; New York: 2001.
63. Desai MP, Labhasetwar V, Walter E, Levy RJ, Amidon GL. Pharm Res 1997;14:1568–1573. [PubMed: 9434276]
64. Esteva FJ. Oncologist 2004;9:4–9. [PubMed: 15163841]
65. Amzel LM, Poljak RJ. Annu Rev Biochem 1979;48:961–997. [PubMed: 89832]
66. Pease LF, Elliott JT, Tsai DH, Zachariah MR, Tarlov MJ. Biotechnol Bioeng 2008;101:1214–1222. [PubMed: 18980182]
67. http://isoeletric.ovh.org
68. Sokolov K, Follen M, Aaron J, Pavlova I, Malpica A, Lotan R, Richards-Kortum R. Cancer Res 2003;63:1999–2004. [PubMed: 12727808]
69. Mauerer M, Penzkofer A, Zweck J. J Photochem Photobiol B 1998;47:68–73.
70. Saxena V, Sadoqi M, Shao J. Int J Pharm 2004;278:293–301. [PubMed: 15196634]
71. Carpenter G. Annu Rev Biochem 1987;56:881–914. [PubMed: 3039909]
72. Yaseen MA, Yu J, Wong MS, Anvari B. Biotechnol Prog 2007;23:1431–1440. [PubMed: 17914861]

73. Huang XH, Jain PK, El-Sayed IH, El-Sayed MA. Photochem Photobiol 2006;82:412–417. [PubMed: 16613493]

74. Gobin AM, Moon JJ, West JL. Int J Nanomed 2008;3:351–358.

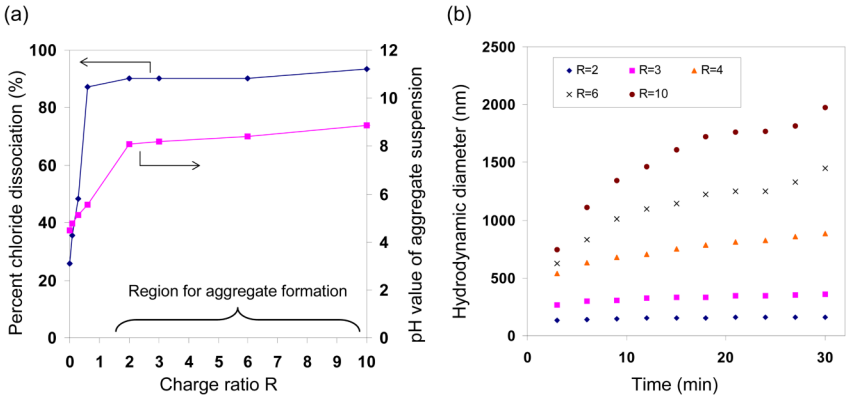

Fig. 1.

(a) Dissociated chloride percentages and corresponding pH values, and (b) hydrodynamic diameters measured for PAH/phosphate aggregate suspensions as functions of *R* ratio. Aggregate formation conditions: temperature = 20 °C, PAH precursor solution concentration of 2 mg/ml, 1:6 volume ratio between PAH and $Na_2HPO_4^{2-}$ precursor solutions.

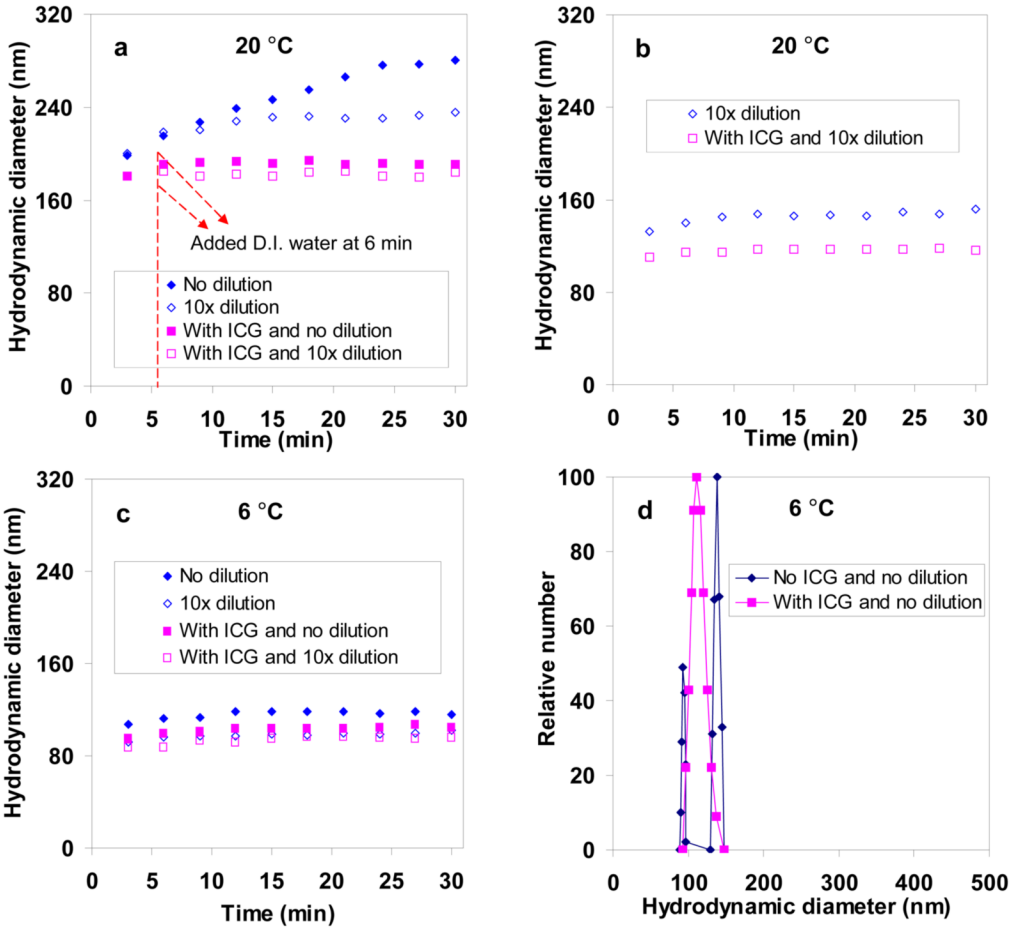

Fig. 2.

DLS study on PAH/phosphate aggregate and PAH/phosphate/ICG aggregate growth behavior (*R*=3) under the effects of 10× dilution and synthesis temperatures: (a) delayed dilution after aggregate formation at 20 °C; (b) immediate dilution after aggregate formation at 20 °C; (c) aggregate formation at 6 °C and the effects of dilution and ICG inclusion; and (d) size distributions at 6 °C and 30 min.

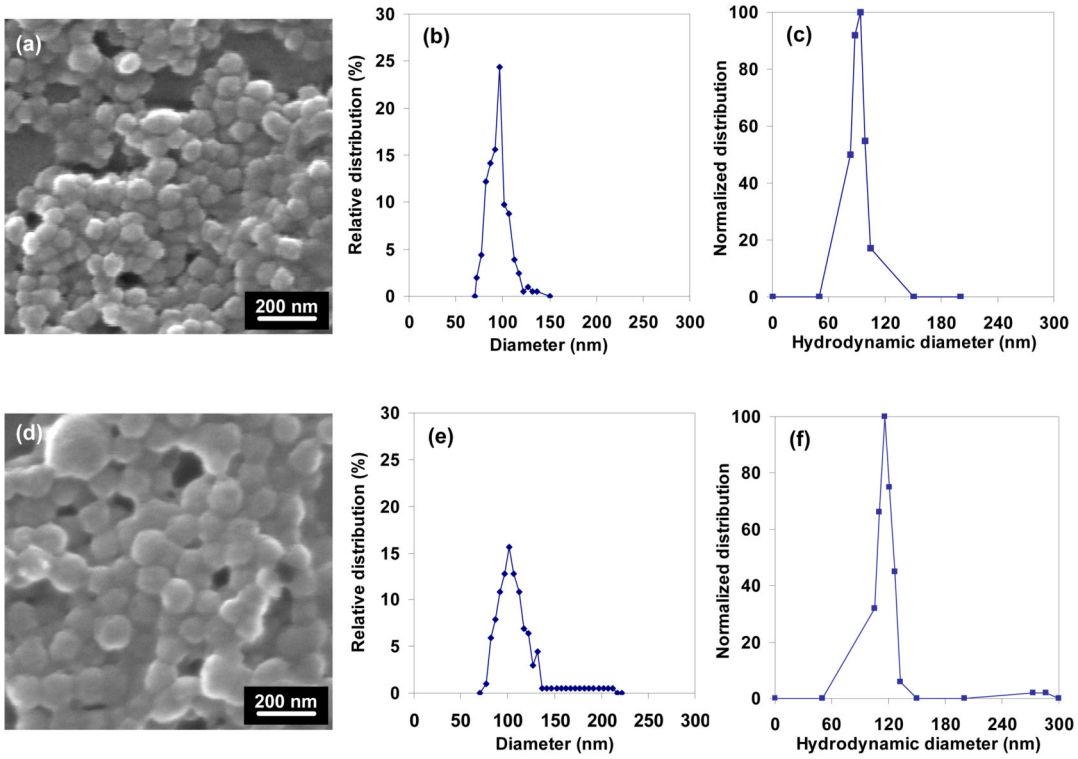

Fig. 3.

(a–c) SEM analysis of uncoated and (d–f) anti-EGFR-coated ICG-containing PAH/phosphate nanocapsules in dried stated: (a, d) SEM images and (b, e) particle size histograms, and (c, f) hydrodynamic diameter distributions of nanocapsules in water.

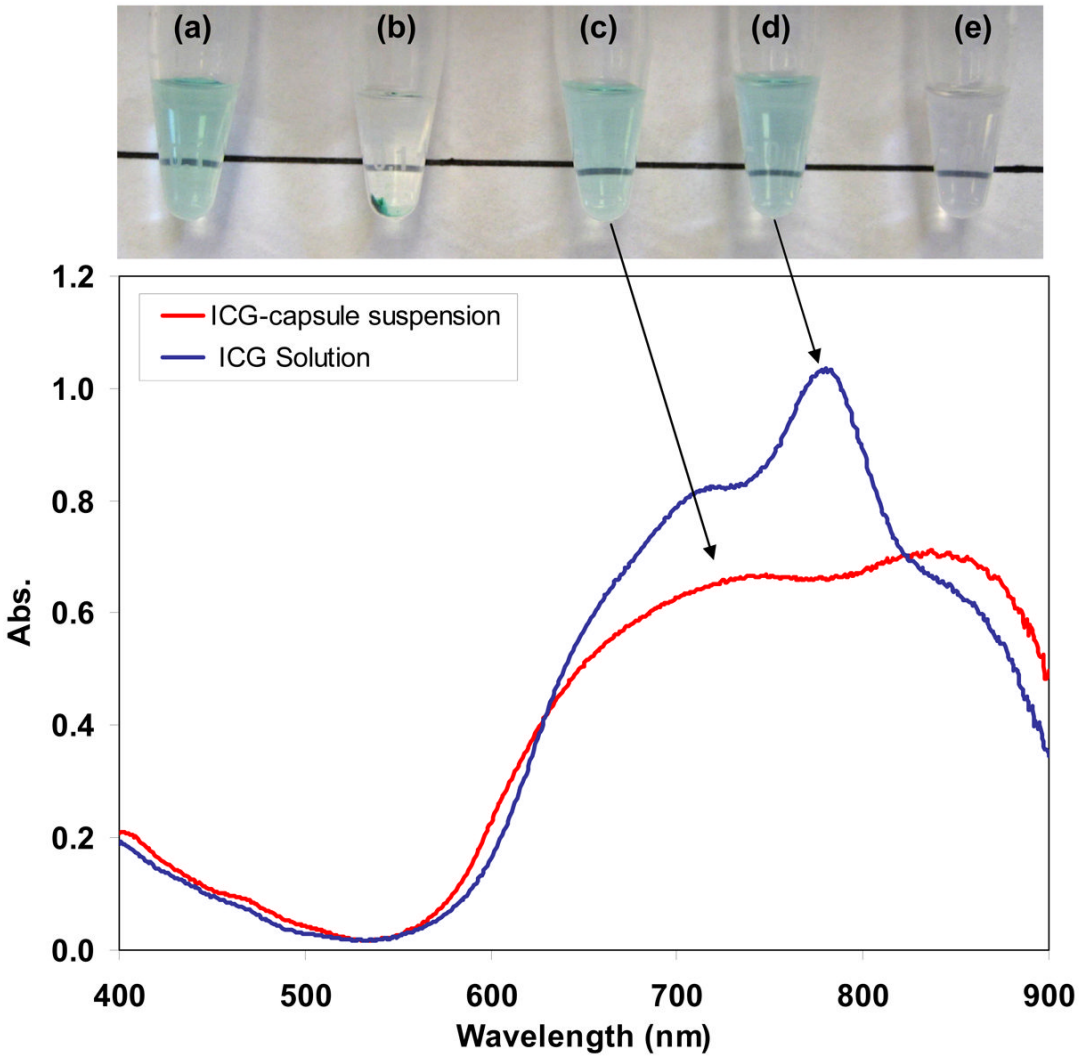

Fig. 4.

Absorbance spectra of non-encapsulated ICG in PBS solution (blue line) and ICG-containing anti-EGFR coated nanocapsule suspension (red line). The ICG concentration was adjusted to 0.03 mg/ml for these formulations (lower than the concentration used in the cell photothermal study). The photographs correspond to anti-EGFR-coated ICG-nanocapsules that (a) are stably suspended in PBS solution, (b) have settled out of suspension, and (c) re-dispersed back into suspension after sonication for 10 sec; (d) non-encapsulated ICG in PBS solution; and (e) a suspension of PAH/HPO_4^{2-} aggregates.

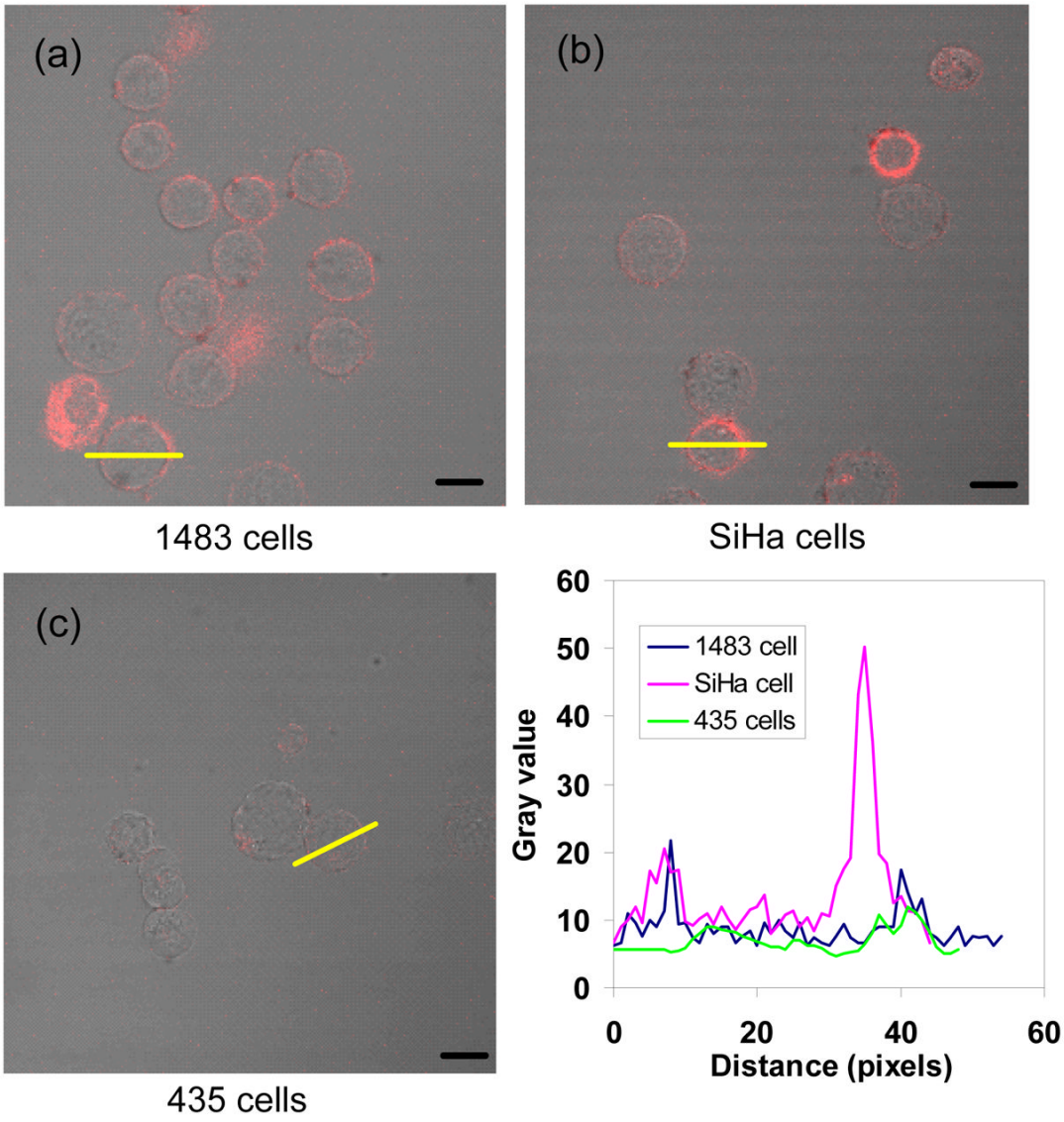

Fig. 5.

Merged brightfield and confocal fluorescence images of (a) 1483, (b) SiHa, and (c) 435 cells incubated with anti-EGFR-coated ICG-containing nanocapsules, and (d) typical fluorescence line intensity profiles shown by the yellow lines in (a), (b), and (c). The incubation time was 30 min at 37°C. Scale bars: 10 μm.

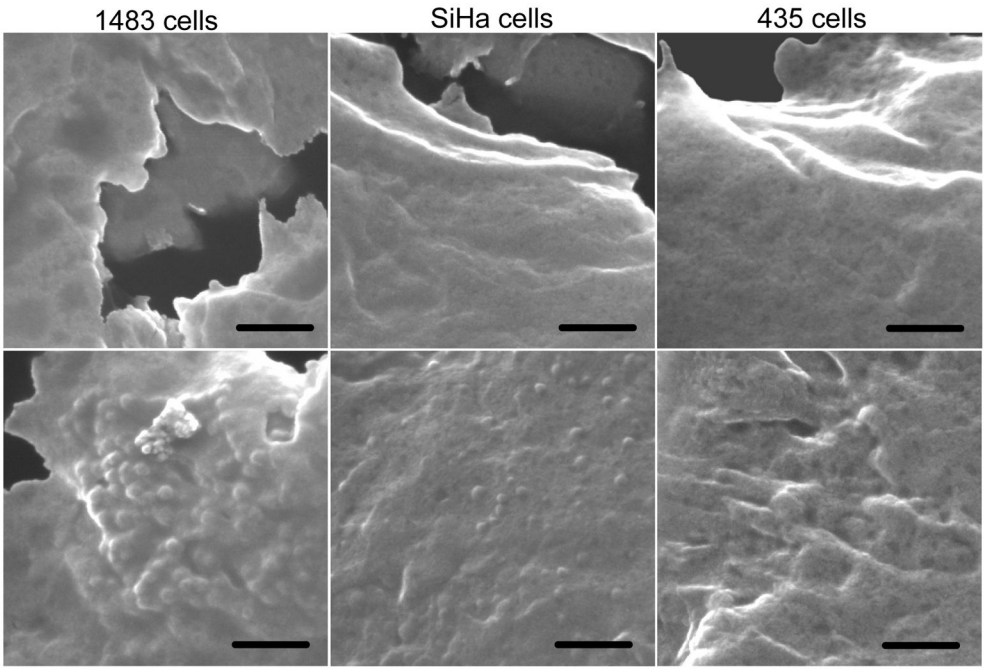

Fig. 6.
SEM images of (a, d) 1483, (b, e) SiHa, and (c, f) 435 cells before (top) and after (bottom) incubation with anti-EGFR-coated ICG-containing nanocapsules. These cells came from the same population that was examined through confocal microscopy. Scale bars: 500 nm.

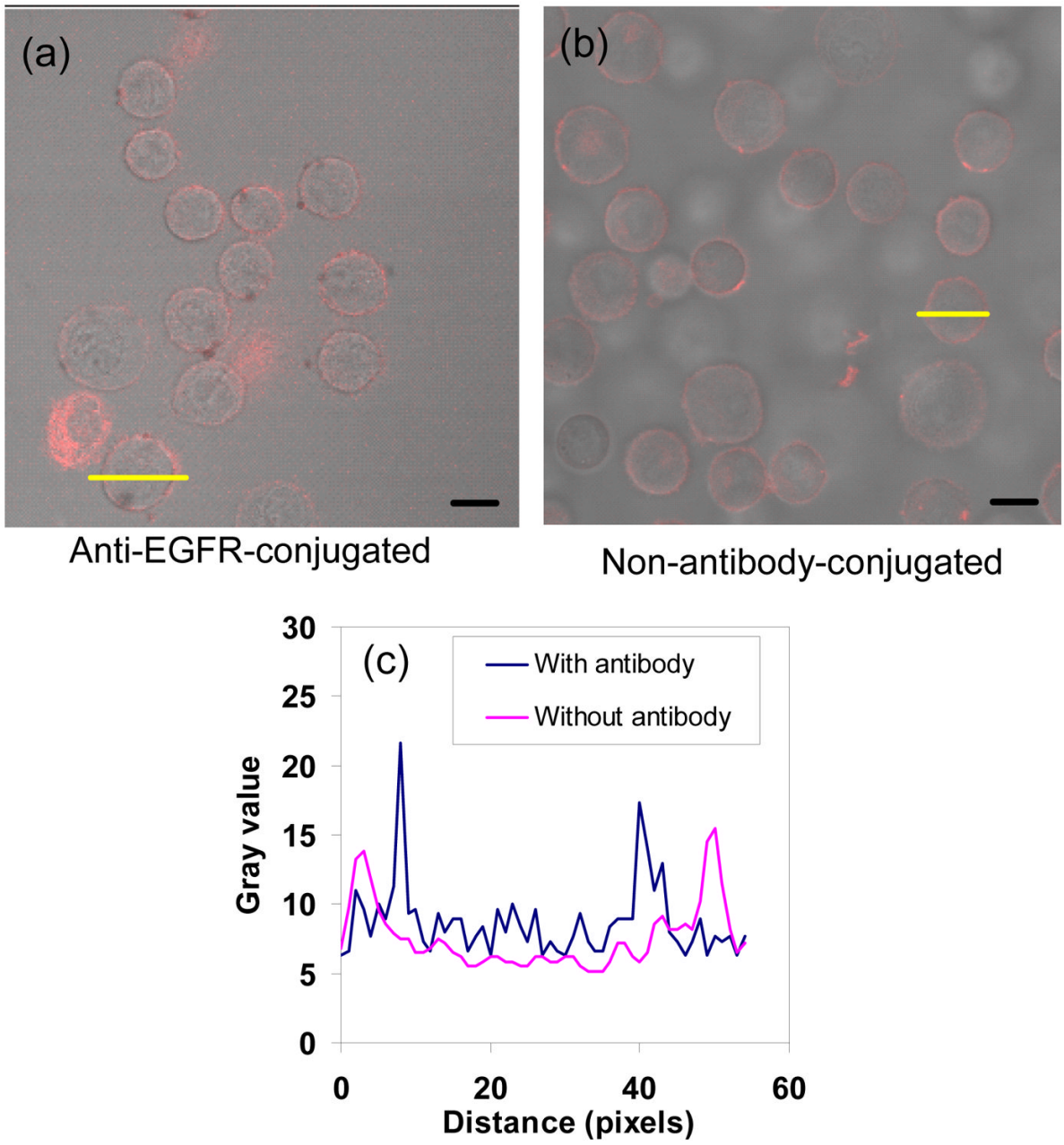

Fig. 7.
Merged brightfield and confocal fluorescence images of 1483 cells incubated with ICG-containing nanocapsules: (a) anti-EGFR-coated and (b) uncoated. (c) Typical fluorescence line intensity profiles shown by the yellow lines in (a) and (b). Scale bars: 10 μm.

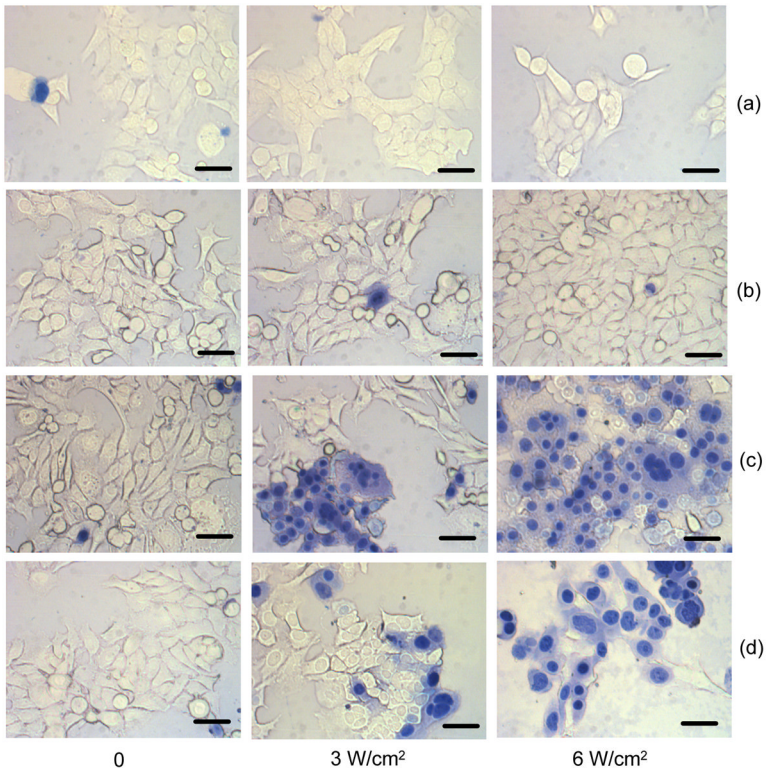

Fig. 8.

Bright field images of 1483 cancer cells incubated with various forms of ICG at 37 °C, optionally irradiated at various radiant exposures, and stained with trypan blue. Images in rows (a)–(d) correspond to cells (a) incubated with no reagents, (b) incubated with free ICG in PBS solution, (c) incubated with anti-EFGR-coated ICG-containing capsules, and (d) incubated with uncoated ICG-containing nanocapsules. ICG solution concentration before exposure to cells was 0.4 mg/ml. 20 μL of ICG sample (either as capsule suspension or in PBS solution) was added to 1 mL of immobilized 1483 cells. The cells were irradiated using an 808-nm continuous wave laser for 200 sec within a 3-mm laser spot. Scale bars: 20 μm.

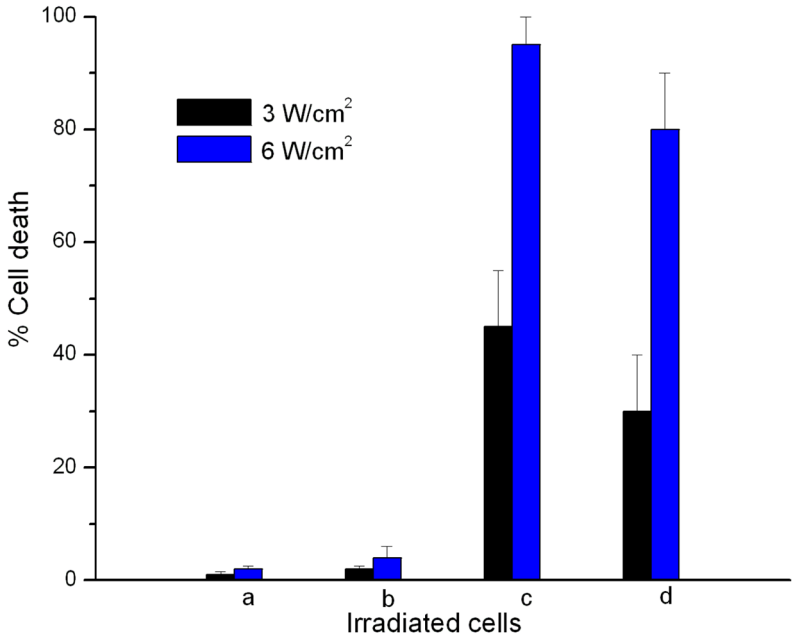

Fig. 9.

Cell death percentage for 1483 cancer cells (a) incubated with no reagents, (b) incubated with free ICG in PBS solution, (c) incubated with anti-EFGR-coated ICG-containing capsules, and (d) incubated with uncoated ICG-containing nanocapsules, in response to laser irradiation (black bars: 3 W/cm^2; blue bars: 6 W/cm^2). Each data point represented 200-cell counts performed on 3 batches of cells, with an error bar of 1 standard deviation.

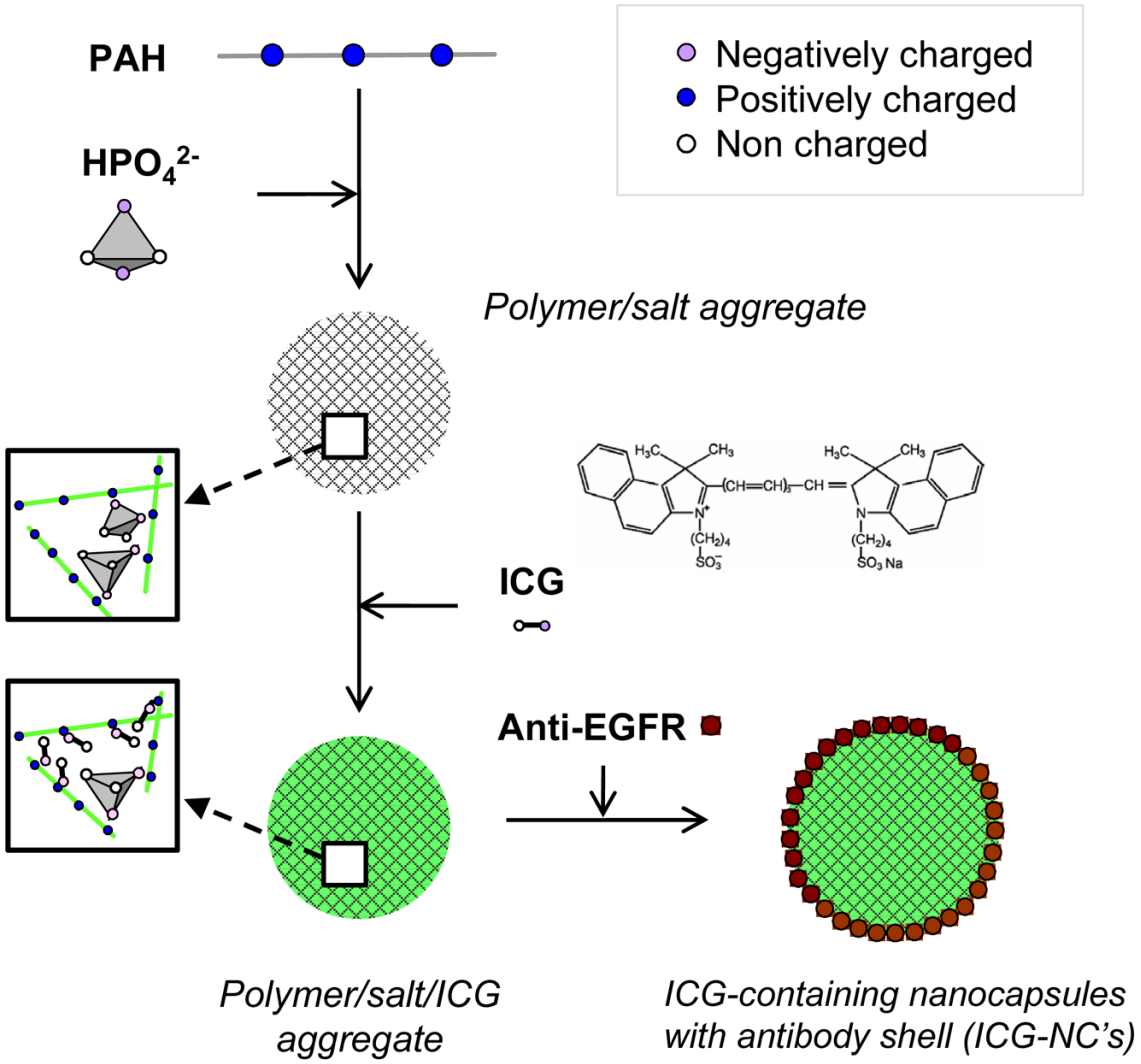

Scheme 1.
Charge-driven tandem, or step-wise, assembly pathway of ICG-containing nanocapsules with anti-EGFR coating.

Table 1

Hydrodynamic diameter measurements of PAH/phosphate aggregates at different aging times. Synthesis conditions: R = 3 and 20 °C.

Time (min)	Intensity-based average diameter (nm)	Relative standard deviation (RSD) (%)	Number-based average diameter (nm)	Relative standard deviation (RSD) (%)	Polydispersity index (PDI)
3	190	3.8	189	3.6	0.005
15	251	5.8	247	5.6	0.032
30	281	13.8	245	11.6	0.06